ISSN 1674-1056
http://cpb.iphy.ac.cn
http://iopscience.iop.org/cpb
中国物理 B
Chinese Physics
中国物理
Chinese Physics B

Compression behavior and spectroscopic properties of insensitive explosive 1,3,5-triamino-2,4,6-trinitrobenzene from dispersion-corrected density functional theory

Yan Su(苏艳), Junyu Fan(范俊宇), Zhaoyang Zheng(郑朝阳), Jijun Zhao(赵纪军), Huajie Song(宋华杰)
Citation: Chin. Phys. B . 2018, 27(5): 056401. **doi:** 10.1088/1674-1056/27/5/056401

Journal homepage: http://cpb.iphy.ac.cn; http://iopscience.iop.org/cpb

What follows is a list of articles you may be interested in

Saturated sodium chloride solution under an external static electric field: A molecular dynamics study

Ren Gan, Wang Yan-Ting
Chin. Phys. B . 2015, 24(12): 126402. **doi:** 10.1088/1674-1056/24/12/126402

Radial collapse and physical mechanism of carbon nanotube with divacancy and 5-8-5 defects

Zhang Ya-Ping, Ling Cui-Cui, Li Gui-Xia, Zhu Hai-Feng, Zhang Meng-Yu
Chin. Phys. B . 2015, 24(4): 046401. **doi:** 10.1088/1674-1056/24/4/046401

Simulations of the flipping images and microparameters of molecular orientations in liquids according to molecule string model

Wang Li-Na, Zhao Xing-Yu, Zhang Li-Li, Huang Yi-Neng
Chin. Phys. B . 2012, 21(8): 086403. **doi:** 10.1088/1674-1056/21/8/086403

Liquid to glass transition of tetrahydrofuran and 2-methyltetrahydrofuran

Tan Rong-Ri, Shen Xin, Hu Lin, Zhang Feng-Shou
Chin. Phys. B . 2012, 21(8): 086402. **doi:** 10.1088/1674-1056/21/8/086402

Temperature dependence of Cu_2O orientations in oxidation of Cu (111)/ZnO (0001) by oxygen plasma

Li Jun-Qiang, Mei Zeng-Xia, Ye Da-Qian, Hou Yao-Nan, Liu Yao-Ping, A. Yu. Kuznetsov, Du Xiao-Long
Chin. Phys. B . 2012, 21(7): 076401. **doi:** 10.1088/1674-1056/21/7/076401

RAPID COMMUNICATION

Compression behavior and spectroscopic properties of insensitive explosive 1,3,5-triamino-2,4,6-trinitrobenzene from dispersion-corrected density functional theory*

Yan Su(苏艳)[1], Junyu Fan(范俊宇)[1], Zhaoyang Zheng(郑朝阳)[2], Jijun Zhao(赵纪军)[1,†], and Huajie Song(宋华杰)[3,‡]

[1] *Key Laboratory of Materials Modification by Laser, Electron, and Ion Beams, Dalian University of Technology, Ministry of Education, Dalian* 116024, *China*

[2] *National Key Laboratory of Shock Wave and Detonation Physics, Institute of Fluid Physics, Chinese Academy of Engineering Physics, Mianyang* 621900, *China*

[3] *Beijing Institute of Applied Physics and Computational Mathematics, Beijing* 100088, *China*

(Received 18 January 2018; revised manuscript received 8 February 2018; published online 26 April 2018)

Using dispersion corrected density functional theory, we systematically examined the pressure effect on crystal structure, cell volume, and band gap of 1,3,5-triamino-2,4,6-trinitrobenzene (TATB) to understand its extraordinary chemical stability. Analysis of the Mulliken population and the electron density of states implied a possible charge transfer in TATB with increasing pressure. Raman and infrared spectra of TATB under hydrostatic pressure up to 30 GPa were simulated. The observed strong coupling between NH_2 groups and NO_2 groups with increasing pressure, which is considered to have a tendency of energy transfer with these vibrational modes, was analyzed. The pressure-induced frequency shift of selected vibrational modes indicated minor changes of molecular conformation mainly by the rotation of NH_2 groups. Compression behavior and spectroscopic property studies are expected to shed light on the physical and chemical properties of TATB on an atomistic scale.

Keywords: 1,3,5-triamino-2,4,6-trinitrobenzene, high-pressure behavior, molecular conformation, Raman spectra

PACS: 64.70.kt, 91.60.Gf, 78.30.–j **DOI:** 10.1088/1674-1056/27/5/056401

1. Introduction

Energetic materials (explosives, propellants, and pyrotechnics) that rapidly detonate and release heat or gaseous products when stimulated by impact or shock have attracted the attention of researchers for several decades because of their wide civilian and military applications.[1,2] Among energetic materials, 1,3,5-triamino-2,4,6-trinitrobenzene (TATB) is a secondary high explosive with extraordinary insensitivity to thermal, impact, or shock stimuli because of its strong intralayer intramolecular and intermolecular hydrogen bond interactions and weak interlayer van der Waals (vdW) interaction.[3] The extended hydrogen bond network of TATB is evidence of its profound chemical stability, especially under high-temperature and high-pressure conditions.

For the safe storage, transport, and use of TATB, it is crucial to elucidate its compression behavior. In this regard, the variations in physical/chemical properties of TATB under high pressure should be characterized, such as polymorphic behavior, decomposition reaction, and detonation process. To date, TATB has been extensively investigated from both theoretical and experimental points of view, especially focusing on its high-pressure behavior. In 1976, Olinger *et al.*[4] obtained the *P*–*V* relationship of TATB under hydrostatic compression by x-ray diffraction. Stevens *et al.*[5] later measured the hydrostatic compression curve of TATB at ambient pressures up to 13 GPa using powder x-ray diffraction in conjunction with a diamond anvil cell.

Infrared and Raman spectroscopies are useful tools to characterize the geometric and bonding features and to disclose the initiation mechanism of shock-compressed energetic materials. Previously, the Raman and IR spectra of TATB crystal under ambient pressure and room temperature, as well as low temperature, have been measured by various groups.[6–8] Under high-pressure conditions, Satija *et al.*[9] reported the effect of static pressure on the Raman spectra of TATB up to 16 GPa. Pravica *et al.*[10] performed an infrared spectroscopic study of TATB and found no phase transition under high pressures up to 10 GPa. Soon thereafter, Pravica *et al.*[11] extended their synchrotron infrared measurements in the mid- and far-IR region up to 40 and 30 GPa, respectively. They found that

*Project supported by the Science Challenge Project of China (Grant No. TZ2016001), the National Natural Science Foundation of China (Grant Nos. 11674046 and 11372053), the Fundamental Research Funds for the Central Universities of China (Grant No. DUT17GF203), the Opening Project of State Key Laboratory of Explosion Science and Technology, Beijing Institute of Technology, China (Grant No. KFJJ16-01M), and the Supercomputing Center of Dalian University of Technology, China.

†Corresponding author. E-mail: zhaojj@dlut.edu.cn

‡Corresponding author. E-mail: song_huajie@iapcm.ac.cn

© 2018 Chinese Physical Society and IOP Publishing Ltd

the peak frequencies of the NH_2 symmetric and antisymmetric modes steadily decreased with increasing pressure, indicating the strengthening of the intermolecular hydrogen bonds. Davidson *et al.*[12] performed Raman spectroscopic analyses on TATB solid and reported an unusually high chemical stability under extremely high static pressures up to 150 GPa, where two subtle structural phase transitions were observed at 28 and 56 GPa. Recently, using *in-situ* Raman spectroscopy and high-speed photography, Saint-Amans[13] investigated the behavior of a TATB-based explosive under shockwave loading up to 30 GPa, in which a complete loss of Raman signal was observed around 9 GPa.

In reality, the detonation process of an energetic material generates a shock wave that represents a high-pressure and high-temperature condition and presents a great challenge for real-time experimental measurement. Alternatively, theoretical calculations provide an effective way to understand the detonation mechanism and decomposition reaction of energetic materials under high pressure and/or high temperature. To date, TATB crystal has been widely explored by *ab initio* calculations based on density functional theory (DFT). Wu *et al.*[14] studied the uniaxial compression effect on the electronic structure of crystalline TATB solid. Liu and co-workers[15,16] investigated the vibrational properties and compression behavior of TATB crystal under hydrostatic pressure up to 10 GPa using DFT within local density approximation and generalized gradient approximation. With PW91, PBE, and local density approximation functionals, Byrd and Rice[17] calculated the crystal structures of five common energetic molecular crystals (including TATB) within the pressure range 0–10 GPa. They pointed out that the disagreement between experimental crystal structures and theoretical results arises from the inadequate description of non-covalent intermolecular interactions by conventional DFT methods. Subsequently, various dispersion correction methods have been implemented into the DFT framework, such as semi-empirical DFT-D[18,19] and non-empirical vdW functionals,[20,21] which provide a better description of the non-covalent interaction of energetic materials. For instance, Sorescu and Rice[22] used DFT-D to further compute the crystallographic properties of 10 energetic molecular crystals including TATB. Their results indicated that the DFT-D method significantly improved the description of intermolecular interactions in molecular crystals under both ambient and high-pressure conditions compared to the conventional DFT. Landerville[23] obtained the equations of state for various energetic materials using DFT calculations with the inclusion of vdW interactions, thermal effects, and zero-point energy corrections, which were able to predict the thermophysical properties of energetic materials within a wide pressure and temperature range. Using the van der Waals-density functional theory (vdW-DFT) approach, Budzevich[24] investigated hydrostatic and uniaxial compressions of TATB and showed that the equilibrium structural and elastic properties and the hydrostatic equations of state were in good agreement with available experimental data. Wu *et al.*[25] performed DFT and DFT-D-based MD simulations to investigate the lattice parameters, electronic structures, and *P*–*V* isotherm of TATB within the pressure range 0–100 GPa at room temperature. Their DFT-D results were consistent with experimental results, but the DFT results without vdW correction misestimated these parameters. They also performed *ab initio* molecular dynamics simulations to investigate the initiation mechanisms and subsequent decompositions of TATB crystal at an initial decomposition temperature of 623 K coupled with different pressures (1–20 GPa).[26] Rykounov[27] systematically considered the pressure effects on the thermodynamic, elastic, and acoustic properties of TATB using dispersion-corrected DFT. Manaa and Fried[28] also observed the nearly equivalent inter- and intramolecular hydrogen bonds within TATB crystal under high pressure. Ojeda and Cagin[29] observed a similar behavior of hydrogen bonds and analyzed the variation of vibrational spectra as a function of pressure.

Despite the extensive theoretical efforts devoted to the pressure effects of TATB, most have focused on the changes of hydrogen bonds and electronic structures. However, the detailed changes in spectroscopic characteristics, possible phase transformations, and the energy transfer mechanism of TATB under extreme conditions are still insufficiently investigated. In this work, we performed dispersion-corrected DFT calculations to examine the changes in crystal/molecular structures and vibrational modes of TATB under pressures of 0–30 GPa. In particular, our simulated Raman and infrared spectra of TATB under high pressure showed minor changes in the molecular conformation at about 3 GPa and 5 GPa.

2. Computational methods

According to x-ray diffraction data, the polymorph of TATB crystal at ambient conditions is a triclinic structure with a $P\bar{1}$ space group.[3] Its unit cell contains two molecules of $C_6H_6N_6O_6$ with a total of 48 atoms (Fig. 1). All DFT calculations within the periodic boundary condition were carried out using the Cambridge Sequential Total Energy Package.[30] The exchange–correlation interaction was treated within the generalized gradient approximation parameterized by the Perdew–Burke–Ernzerhof (PBE) functional.[31] Norm-conserving pseudopotentials were used to describe the ion-electron interactions.[32] From our previous benchmark calculations,[33] it was confirmed that intermolecular non-covalent interactions play a significant role in energetic molecular crystals and must be properly accounted for. Thus, the empirical dispersion correction scheme by Grimme,[19] PBE-D2, was employed to describe the non-covalent interactions. As a compromise between computational cost and accuracy, a $2\times2\times2$ Monkhorst–Pack k grid for sampling the Brillouin zones[34] and a kinetic energy cutoff of 1000 eV for plane-wave basis were adopted. The unit cell parameters and atomic

coordinates were fully relaxed by the Broyden, Fletcher, Goldfarb, and Shannon algorithm.[35] The convergence criteria of maximum total energies of 5×10^{-6} eV/atom, the maximum force of 0.01 eV/Å, the maximum stress of 0.02 GPa, and the maximum displacement of 5×10^{-4} Å were employed throughout all calculations. Hydrostatic pressure was applied from 0 to 30 GPa in steps of 0.5 GPa.

Based on the optimized crystal structures, Raman and infrared spectra were computed with the density functional perturbation theory.[36] Intensities of Raman peaks were calculated by the linear response formalism. The experimental factors of temperature (10 K) and incident light wavelength (514.5 nm) were taken into account for simulating the Raman intensity. The spectrum peak was broadened by a 20-cm^{-1} wide Lorentzian functional.

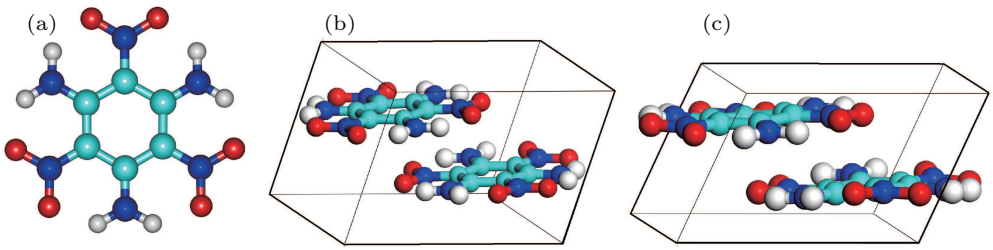


Fig. 1. (color online) (a) Molecular structure of TATB ($C_6H_6N_6O_6$) and crystal structures of TATB crystal at (b) 0 GPa and (c) 30 GPa. Color scheme: C, green; N, blue; O, red; H, white.

3. Results and discussion

First, we optimize the lattice parameters of TATB crystal at zero pressure and compare them with the experimental XRD data and previous DFT calculations with and without dispersion correction. As shown in Table 1, our computed lattice parameters were reasonably close to the experimental values,[3] that is, lattice parameters a and b were overestimated by 1.19% and 1.12%, respectively, while the lattice parameter c and unit cell volume V were underestimated by 2.68% and 1.11%, respectively. After a comprehensive assessment of lattice constants and lattice angles, the current PBE-D2 scheme provided more reasonable and accurate results than the previous computational results,[16,17,22,24,28] especially for those from pure DFT calculations. However, it should be noted that the computed lattice constant of the c axis had a relatively large deviation from the measured value by 0.18 Å, suggesting that DFT-D2 is not accurate for describing the interlayer vdW interaction.

Table 1. Comparison of experimental (Ref. [3]) and computational (DFT-D2) lattice parameters and unit cell volumes V of TATB crystal at zero pressure.

Cell parameter	a/Å	b/Å	c/Å	α/(°)	β/(°)	γ/(°)	V/Å^3
Exp.[3]	9.010	9.028	6.812	108.59	91.82	119.97	442.49
DFT-D2	9.118	9.129	6.629	109.54	91.52	119.98	437.57
Error/%	1.19	1.12	2.68	0.87	0.32	0.01	1.11

Figure 2 shows the variation of lattice parameters as a function of pressure up to 30 GPa. Overall, the lattice parameters of TATB crystal from our theoretical calculation are in reasonable accordance with experimental data[4] and previous calculations.[17,27] Our computed lattice parameter c was consistent with the experimental data[4] and our DFT-D result[27] was better than the pure DFT result,[17] further confirming the importance of dispersion correction within DFT for describing the weak interlayer interaction in TATB along the c axis. In Fig. 2, note that lattice parameters a and b exhibited a nearly identical decrease with increasing pressure, whereas the lattice parameter c reduced drastically with increasing pressure. This can be explained by the fact that the weaker interlayer vdW interaction along the c axis is more compressible than the relatively stronger hydrogen bonds within the ab plane. Figure 2 also shows the pressure-induced volume compression V/V_0 of TATB up to 30 GPa, together with previous experimental[4] and computational[17,27] results. Similar to the lattice parameters, our DFT-D2 calculations approximately reproduced the trend of pressure-induced reduction of volume by experiment, in which the volume reduction V/V_0 at up to 30 GPa was 67%.

We further examined the changes of molecular conformation in a TATB crystal under high pressure. With increasing pressure, the TATB molecules gradually approached each other and transformed from a flat to a curved configuration because of the large compressible intermolecular spacing, significant intralayer hydrogen bonds, and weak interlayer vdW interaction as shown in Figs. 1(b) and 1(c). Figure 3 displays the pressure dependences of the bond lengths for two C–N bonds (both nitro and amino) and the intramolecular and intermolecular hydrogen bonds of the amino and nitro groups. The lengths of intermolecular hydrogen bonds N–H$\cdots$O–N between adjacent molecules decreased continuously with a compression rate of -0.018 Å/GPa. In contrast, the bond lengths of two C–N bonds and intramolecular hydrogen bonds N–H$\cdots$O–N between the hydrogen of the amino and the oxygen of the nitro group showed little pressure-induced change within the entire pressure range, i.e., compression rates of about -0.0018 Å/GPa, -0.0011 Å/GPa (C–N bonds of nitro

and amino), and −0.0019 Å/GPa (N–H···O–N of intra), respectively. The intermolecular hydrogen bond decreased from about 2.33 Å at 0 GPa to 1.80 Å at 30 GPa with a noticeable 0.53 Å reduction of amplitude. In contrast, the intramolecular bond changed by only 0.06 Å within the same pressure range (i.e., from about 1.71 Å at 0 GPa to 1.65 Å at 30 GPa), indicating a much stronger compression of the intermolecular hydrogen bonds.

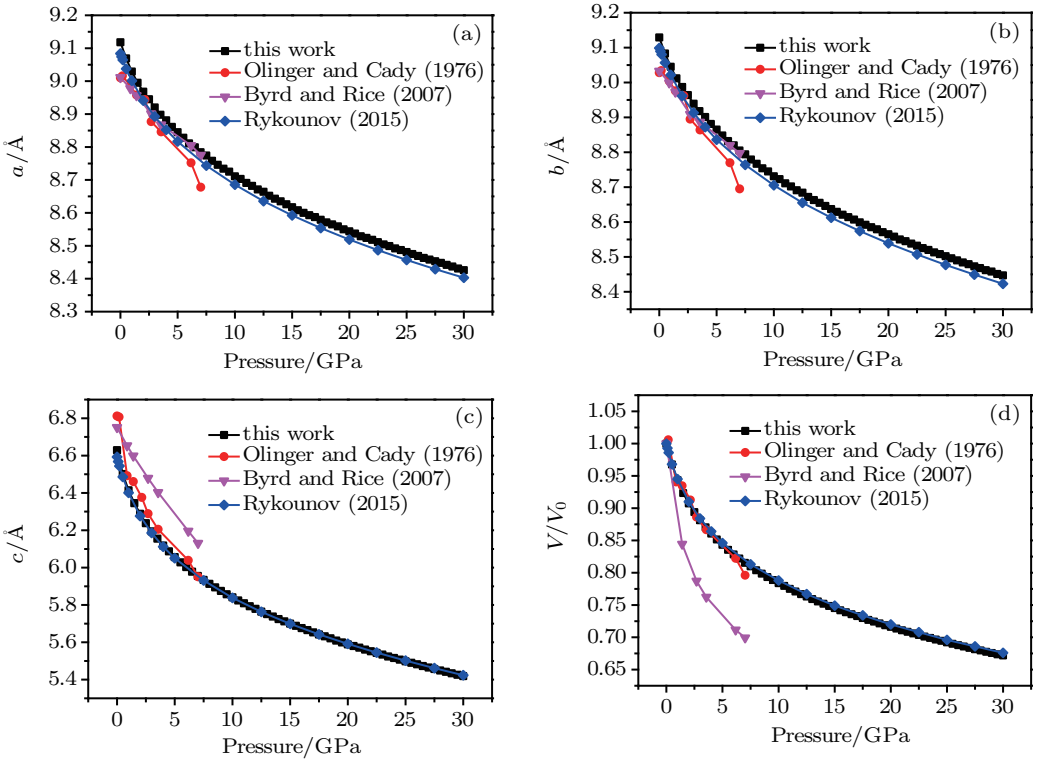


Fig. 2. (color online) (a)–(c) Lattice parameters and (d) unit cell volume compression V/V_0 of TATB crystal as a function of pressure. Experimental results are from Ref. [4] and computational results are from Refs. [17] and [27].

Mulliken population analysis further supports the trend of bond variations and reveals the pressure-induced charge transfer in TATB. As shown in Table 2, as pressure increases, the on-site charges of amino H, amino C, nitro N, and nitro O continuously increased, whereas the on-site charges of nitro C and amino N were significantly reduced. Overall, under external pressure, charges are transferred from the amino group to the nitro group; the average charges on the amino and nitro group were $-0.044|e|$ and $-0.002|e|$, respectively, at zero pressure, while they became $-0.005|e|$ and $-0.007|e|$ at 30 GPa, respectively. Variation of the covalent bond lengths with pressure affects the charge density distributions as demonstrated in Fig. 4. Enhanced interactions in the intra- and intermolecular hydrogen bonds are clearly seen from the contour plots in Fig. 4. In particular, the overlap of electron densities between amino H and the nearest neighboring nitro O in TATB increase with increasing pressure, indicating the occurrence of inter-group charge transfer.

Table 2. Mulliken charges (e) on every atom of TATB crystal under 0, 15, and 30 GPa.

Pressure	C (NH_2)	N (NH_2)	H(NH_2)	C (NO_2)	N (NO_2)	O (NO_2)
0 GPa	0.203	–0.707	0.460	0.053	0.360	–0.415
15 GPa	0.203	–0.647	0.435	0.067	0.350	–0.421
30 GPa	0.196	–0.616	0.425	0.073	0.343	–0.423

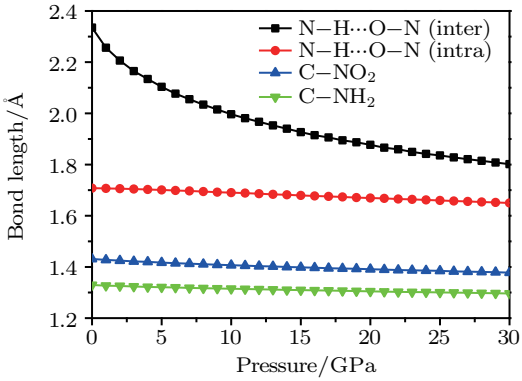


Fig. 3. (color online) Evolution of bond lengths of two C–N bonds (both nitro and amino) and intramolecular and intermolecular hydrogen bonds of amino and nitro groups with pressure.

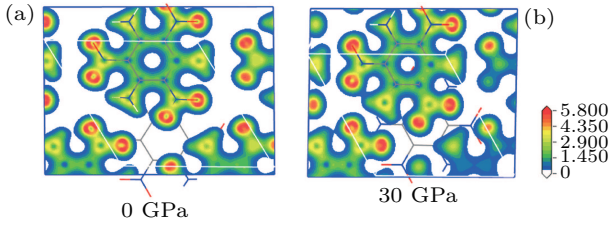


Fig. 4. (color online) Contour plots of charge density distribution of TATB crystal under (a) 0 and (b) 30 GPa.

In addition, the pressure-induced shrinkage of bond

lengths results in a variation of the band gap and increases the sensitivity of energetic materials because a decreasing band gap leads to increased impact sensitivity.[37] Table 3 presents the band gaps of TATB crystal under selected pressures. As the pressure increased, the band gap of TATB gradually decreased, which was also observed in Wu's calculations.[25] This can be ascribed to the decrease of intermolecular spacing under compression leading to the approaching of different groups and charge density overlap and electron delocalization. At up to 30 GPa, the compressed TATB crystal had an appreciable band gap of 1.61 eV, indicating high chemical stability. Note that there is no structural phase transition in TATB within the considered pressure region from both our theoretical calculations and experiments.[12] In contrast, most energetic materials undergo amorphization or phase transformation at relatively low pressures as well as band gap closure; for example, FOX-7 exhibits a molecular conformational change at 2 GPa and a structural phase transition at 4.5 GPa.[38]

The electronic structures of the compressed TATB crystal can be further analyzed by the partial density of states (PDOS) and total density of states. Figure 5 shows the PDOS for TATB under 0 and 30 GPa. One can see that the 2p states of O, C, and amino N atoms contribute mostly to the conduction bands, while the 2p states of O, C, and nitro N atoms dominate the valence bands near the Fermi level. Therefore, we suggest that the nitro O atom and amino N atom mainly contribute to the relative reactivity of TATB under shock, which coincides well with the experimental and computational results showing that the loss of oxygen is assisted by an intramolecular/intermolecular NH_2 group of TATB under external stimuli.[39–41] Under 30 GPa, the variation of the PDOS for the O atom is more pronounced than the other atoms, verifying the possible charge transfer from the amino group to the nitro group in TATB.

Table 3. Band gaps (eV) of TATB crystal under pressures of 0, 10, 20, and 30 GPa from this calculation (DFT-D2) and Ref. [25] (DFT-D).

Pressure	0 GPa	10 GPa	20 GPa	30 GPa
DFT-D2	2.36	1.97	1.77	1.61
DFT-D	2.60	2.16	1.97	1.73

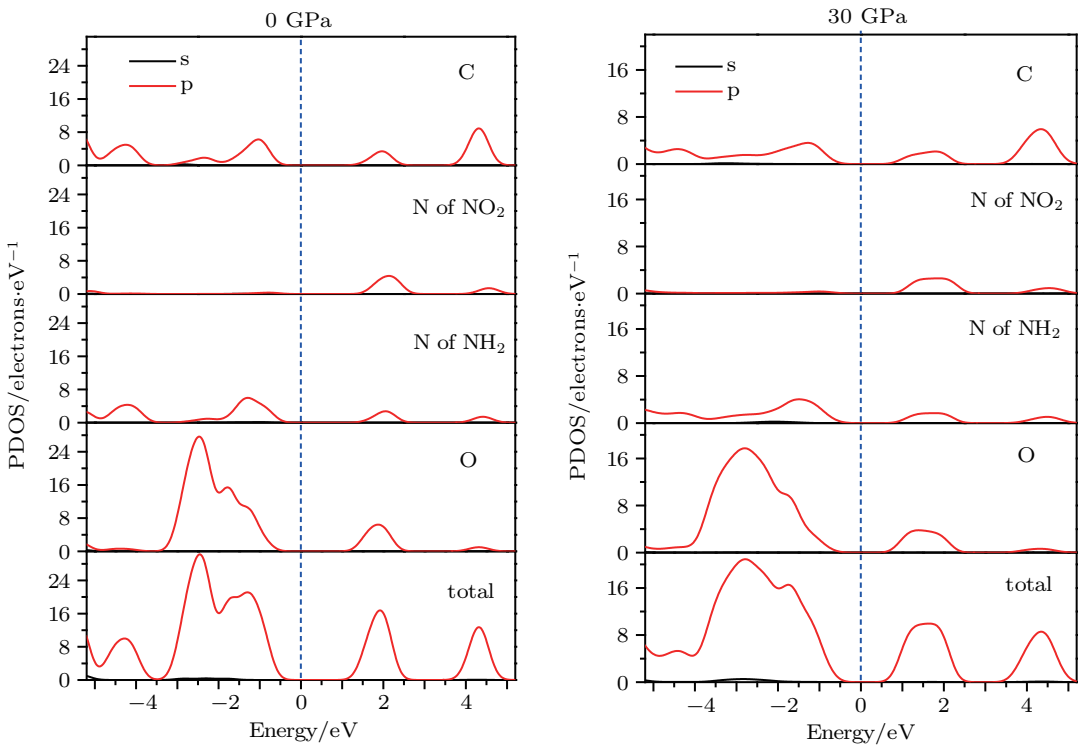


Fig. 5. (color online) Partial density of states of TATB at (a) 0 and (b) 30 GPa. The blue vertical dotted line indicates the Fermi level.

Raman and infrared spectra are critical for understanding the strength of chemical bonds, intermolecular interactions, and vibrational coupling of a molecular crystal at high pressure. Thus, vibrational frequencies of Raman and infrared spectra for TATB under hydrostatic compression were calculated and analyzed. Table 4 lists the computed vibrational frequencies of TATB crystal and the assignment to different modes, together with previously measured data at ambient pressure.[7] Our computational frequencies excellently reproduced the experimental peak positions in which the mean square error of frequency was only 9 cm^{-1}. Figure 6(a) displays the evolution of Raman spectra of TATB as a function of pressure over a broad frequency range. The lower frequency peaks below approximately 200 cm^{-1}, including internal modes and lattice modes, corresponding to the skeletal deformation of TATB. The intermediate frequency modes in the range 200–1600 cm^{-1} have a rather complicated character and mainly consist of C–NH_2 stretching, NO_2 stretching and scis-

soring, C–NO_2 twisting, and NH_2 scissoring, wagging, and rocking modes. The highest frequency modes in the range 3200–3400 cm^{-1} have been assigned to the symmetric and asymmetric NH_2 stretching vibrations. As seen in Fig. 6(a), most vibrational frequencies shift gradually toward higher frequencies (i.e., blue shift) with increasing pressure as a result of the reduced interatomic distances, except for the NH_2 rocking vibration mode. This behavior is consistent with previous high-pressure Raman experiments of TATB crystals.[13] The observed blue shift of most vibrational frequencies is caused by the strengthening of chemical bonds, especially the inter- and intramolecular hydrogen bonds enhanced by compression.

Table 4. Calculated and experimental vibrational frequencies (in cm^{-1}) of TATB crystal at ambient pressure.

Mode	This work	Exp.[7]	Assignment
M1	3346		NH_2 asym. stretch
M2	3343		NH_2 asym. stretch
M3	3333	3302	NH_2 asym. stretch
M4	3236		NH_2 sym. stretch
M5	3227	3213	NH_2 sym. stretch
M6	3220	3203	NH_2 sym. stretch
M7	1554	1566	C–NH_2 stretch
M8	1545		C–NH_2 stretch
M9	1535	1526	C–NH_2 stretch
M10	1498	1493	NH_2 scissor
M11	1492	1485	NH_2 scissor
M12	1437	1430	NH_2 scissor
M13	1437	1420	NH_2 scissor
M14	1394	1378	NH_2 scissor + C–NO_2 stretch + Ring breath
M15	1374	1368	NH_2 scissor + NO_2 asym. stretch
M16	1344	1341	Ring stretch + NH_2 rock
M17	1286		NH_2 scissor
M18	1280	1279	NH_2 scissor
M19	1199		Ring breath + NO_2 stretch + NH_2 scissor
M20	1196		Ring stretch + NO_2 stretch + NH_2 scissor
M21	1192	1191	Ring stretch + NO_2 stretch + NH_2 stretch
M22	1149	1144	NH_2 scissor
M23	1147		NO_2 stretch + NH_2 scissor
M24	1120	1134	NH_2 rock + C–NH_2 stretch
M25	1114		NH_2 rock
M26	1027	1028	NH_2 rock
M27	1026	1023	NH_2 rock
M28	864	874	NO_2 stretch + NH_2 rock
M29	862	878	NO_2 stretch + NH_2 rock
M30	831	833	NH_2 twist
M31	820	818	NH_2 twist
M32	814	811	NH_2 twist
M33	808	806	NH_2 twist + NO_2 stretch
M34	777	780	NH_2 wag
M35	763	761	NH_2 wag + ring wag
M36	744	749	NH_2 wag
M37	730	729	NH_2 twist
M38	726	729	NH_2 wag
M39	715	709	NH_2 wag
M40	696	696	NO_2 scissor + NH_2 rock
M41	695		C–NH_2 stretch + C–NO_2 scissor
M42	694		NH_2 rock
M43	680	670	C–NH_2 wag + C–NO_2 wag
M44	646		C–NH_2 wag
M45	645		C–NH_2 wag
M46	605	614	C–NH_2 stretch
M47	511		NH_2 rock + NO_2 rock
M48	511	506	NH_2 rock
M49	490		NH_2 rock + NO_2 rock
M50	441	449	NH_2 rock + NO_2 rock
M51	440	445	NH_2 rock
M52	391	390	NH_2 rock + NO_2 rock
M53	384		C–NO_2 stretch
M54	367	370	C–NH_2 stretch + C–NO_2 rock
M55	364	369	C–NH_2 stretch + C–NO_2 twist
M56	338	333	NH_2 twist
M57	331	332	NH_2 twist
M58	289	297	C–NH_2 stretch + C–NO_2 twist
M59	288	296	C–NH_2 stretch + C–NO_2 twist
M60	225	231	C–NH_2 wag

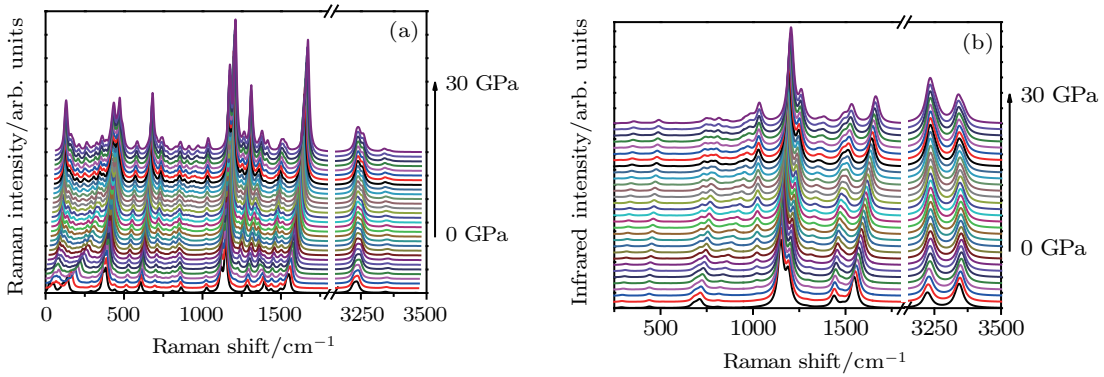


Fig. 6. (color online) Variations of simulated (a) Raman and (b) infrared spectra with pressure (0–30 GPa) over a broad frequency range.

To further illustrate the pressure-dependent change of vibrational frequencies, the peak positions for selected modes as a function of pressure are depicted in Fig. 7. Interestingly, some abnormal frequency changes for a few vibrational modes are observed at pressures around 3 and 5 GPa, whereas the experimental Raman spectra of TATB revealed no phase transition up to at least 28 GPa.[12] Nonetheless, our DFT-D calculations also show that the crystal structure is basically retained and there is no phase change within the pressure range 0–30 GPa. Thus, the abnormal Raman frequency changes are attributed to minor changes in molecular conformation, mainly because of the rotation of the NH_2 groups of TATB. Specifically, the NH_2 groups of TATB continuously undergo distortions and rotations and move away from their original locations under the compression process but exhibit reverse twisting around 3 and 5 GPa, triggering abnormal frequency changes.

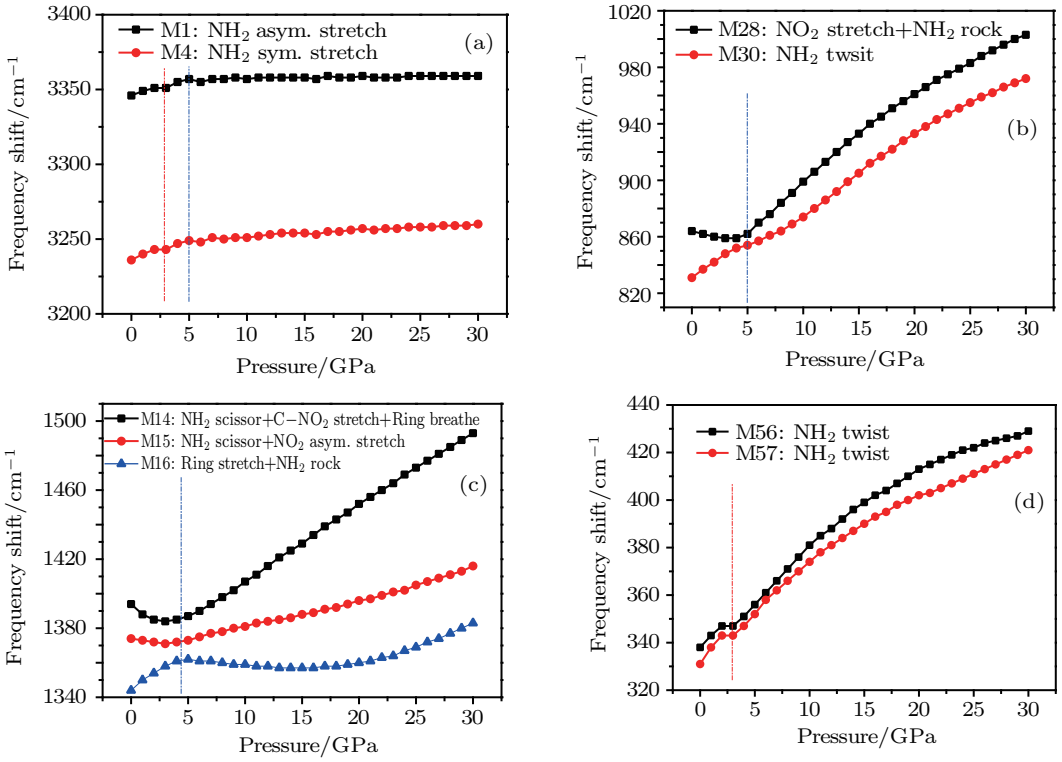


Fig. 7. (color online) Pressure-induced frequency shift of selected Raman frequency modes (see Table 4 for definition).

Further analysis shows that the frequencies for NH_2 stretching (M1, M4) and NH_2 twisting (M30, M56, M57) modes monotonically increase with increasing pressure, both showing a subtle saltation around 3 GPa. In addition, NH_2 stretching frequencies present minor changes at about 5 GPa. More complex behaviors were observed for other modes. Modes 14, 15, and 28 contributed NH_2 scissoring, NH_2 rocking, and NO_2 stretching vibrations, respectively, a gradual red shift at less than 5 GPa, and a blue shift with increasing pressure. In particular, with increasing pressure, the vibrational character of pure NH_2 scissoring mode 14 was gradually mixed with C–NO_2 stretching and ring breathing vi-

brations, whereas the combinational mode 28 included less NO_2 stretching vibrations and gradually became a pure NH_2 rocking vibration. All these behaviors reveal strong coupling between NO_2 and NH_2 groups resulting from intra- and intermolecular hydrogen bonds and imply a transfer of energy among these vibrational modes. In contrast, as the pressure increases, the frequency of mode 16 consisting of NH_2 rocking and ring stretching first rose at a pressure less than 5 GPa and then dropped at up to 15 GPa. Meanwhile, it should be emphasized that there is no crossing of Raman vibrational peaks of these modes under all pressures up to 30 GPa. Similar behaviors were observed in the simulated infrared spectra of TATB in Fig. 6(b), showing as pressure-dependent anomalous spinodal around 3 and 5 GPa.

4. Conclusion

We carried out systematical DFT calculations to gain insight into the high-pressure molecular conformations and spectroscopic characters of the TATB insensitive explosive. Compared with the available experimental data and previous DFT calculations, it was shown that dispersion-corrected DFT is necessary to describe the TATB crystal. Under hydrostatic pressures up to 30 GPa, the changes of the lattice structure, cell volume, and the electronic band gap of TATB suggest unusually high chemical stability. Mulliken population analysis and density of states of TATB reveal possible charge transfer from NH_2 groups to NO_2 groups with increasing pressure. The simulated Raman and infrared spectra of TATB indicate the strengthening of hydrogen bonds and a strong coupling between NO_2 and NH_2 groups. Abnormal changes of selected vibrational modes are also observed at approximately 3 and 5 GPa, which are associated with minor changes of molecular conformation without changes in crystal symmetry. The present study provides a comprehensive understanding of the pressure dependence of crystal structures and vibrational spectra of insensitive energetic crystal, and may trigger further experiments to explore the high-pressure behavior of TATB and other energetic materials.

References

[1] Sikder A K, Maddala G, Agrawal J P and Singh H 2001 *J. Hazard. Mater.* **84** 1

[2] Badgujar D M, Talawar M B, Asthana S N and Mahulikar P P 2008 *J. Hazard. Mater.* **15** 289

[3] Cady H H and Larson A C 1965 *Acta Crystallogr.* **18** 485

[4] Olinger B W and Cady H H 1976 in *Proceedings: Sixth International Symposium on Detonation, Coronado, California*, USA, August 24–27, p. 224

[5] Stevens L L, Velisavljevic N, Hooks D E and Dattelbaum D M 2008 *Propell. Explos. Pyrot.* **33** 286

[6] Vergoten G, Fleury G, Blain M and Odiot S 1985 *J. Raman Spectrosc.* **16** 143

[7] McGrane S D and Shreve A P 2003 *J. Chem. Phys.* **119** 5834

[8] McGrane S D, Barber J and Quenneville J 2005 *J. Phys. Chem. A* **109** 9919

[9] Satija S K, Swanson B, Eckert J and Goldstone J A 1991 *J. Phys. Chem.* **95** 10103

[10] Pravica M, Yulga B, Liu Z X and Tschauner O 2007 *Phys. Rev. B* **76** 064102

[11] Pravica M, Yulga B, Tkachev S and Liu Z X 2009 *J. Phys. Chem. A* **113** 9133

[12] Davidson A J, Dias R, Dattelbaum D and Yoo C 2011 *J. Chem. Phys.* **135** 174507

[13] Saint-Amans C, Hebert P, Doucet M and de Resseguier T 2015 *J. Appl. Phys.* **117** 023102

[14] Wu C J, Yang L H and Fried L E 2003 *Phys. Rev. B* **67** 235101

[15] Liu H, Zhao J J, Ji G F, Wei D Q and Gong Z Z 2006 *Phys. Lett. A* **358** 63

[16] Liu H, Zhao J J, Du J G, Gong Z Z, Ji G F and Wei D Q 2007 *Phys. Lett. A* **367** 383

[17] Byrd E F C and Rice B M 2007 *J. Phys. Chem. C* **111** 2787

[18] Grimme S 2004 *J. Comput. Chem.* **25** 1463

[19] Grimme S 2006 *J. Comput. Chem.* **27** 1787

[20] Dion M, Rydberg H, Schroder E, Langreth D C and Lundqvist B I 2004 *Phys. Rev. Lett.* **92** 246401

[21] Neumann M A and Perrin M A 2005 *J. Phys. Chem. B* **109** 15531

[22] Sorescu D C and Rice B M 2010 *J. Phys. Chem. C* **114** 6734

[23] Landerville A C, Conroy M W, Budzevich M M, Lin Y, White C T and Oleynik I I 2010 *Appl. Phys. Lett.* **97** 251908

[24] Budzevich M M, Landerville A C, Conroy M W, Lin Y, Oleynik I I and White C T 2010 *J. Appl. Phys.* **107** 113524

[25] Wu Q, Zhu W H and Xiao H M 2014 *RSC Adv.* **4** 53149

[26] Wu Q, Chen H, Xiong G L, Zhu W H and Xiao H M 2015 *J. Phys. Chem. C* **119** 16500

[27] Rykounov A A 2015 *J. Appl. Phys.* **117** 215901

[28] Manaa M R and Fried L E 2012 *J. Phys. Chem. C* **116** 2116

[29] Ojeda O U and Cagin T 2011 *J. Phys. Chem. B* **115** 12085

[30] Segall M D, Lindan P J D, Probert M J, Pickard C J, Hasnip P J, Clark S J and Payne M C 2002 *J. Phys.: Condens. Matter* **14** 2717

[31] Perdew J P, Burke K and Ernzerhof M 1996 *Phys. Rev. Lett.* **77** 3865

[32] Hamann D, Schlüter M and Chiang C 1979 *Phy. Rev. Lett.* **43** 1494

[33] Fan J Y, Zheng Z Y, Su Y and Zhao J J 2017 *Mol. Simul.* **43** 568

[34] Monkhorst H J and Pack J D 1976 *Phys. Rev. B* **13** 5188

[35] Fischer T H and Almlof J 1992 *J. Phys. Chem.* **96** 9768

[36] Refson K, Clark S J and Tulip P R 2006 *Phys. Rev. B* **73** 155114

[37] Zhu W H and Xiao H M 2010 *Struct. Chem.* **21** 657

[38] Dreger Z A, Tao Y C and Gupta Y M 2014 *J. Phys. Chem. A* **118** 5002

[39] Östmark H 1995 *AIP Conf. Proc.* **370** 871

[40] He Z H, Chen J and Wu Q 2017 *J. Phys. Chem. C* **121** 8227

[41] Tiwari S C, Nomura K, Kalia R K, Nakano A and Vashishta P 2017 *J. Phys. Chem. C* **121** 16029